

# **Nonlinear Optics (WiSe 2017/18)**

## **Lecture 24: January 23, 2018**

### **12 High-harmonic generation and attoscience**

#### **12.3 Attosecond pulses**

12.3.6 RABBITT, attosecond streaking, FROG-CRAB

12.3.7 Transient XUV absorption spectroscopy

12.3.8 Attosecond ion-charge-state chronoscopy

12.3.9 Multi-purpose attoscience beamlines

# Nonlinear Optics (WiSe 2017/18)

## Lecture 24: January 23, 2018

### 13 Strong-field physics in solids

#### 13.1 Prototype examples: the semiconductors GaAs and ZnO

#### 13.2 Energy scales of light-matter interactions in solids

##### 13.2.1 Rabi energy

##### 13.2.2 Ponderomotive energy

##### 13.2.3 Bloch energy

#### 13.3 Semiconductor Bloch equations

(13.4 Carrier-wave Rabi flopping)

(13.5 THG in disguise of SHG)

} in Lecture 19 already

#### 13.6 High-harmonic generation from solids

# FROG-CRAB

Frequency-Resolved Optical Gating for Complete Retrieval of Attosecond Bursts  
Y. Mairesse and F. Quéré, Phys. Rev. A 71, 011401 (2005)

In [69, 70], the deep connection between RABBITT and attosecond streaking was revealed and unified to the more general FROG-CRAB technique. Within the framework of the strong-field approximation (SFA) [7, 3], the transition amplitude to the final continuum state  $|\mathbf{v}\rangle$  of the electron with momentum  $\mathbf{v}$  can be expressed as [70]

$$a(\mathbf{v}, \Delta t) = -i \int_{-\infty}^{+\infty} dt e^{i\phi(t)} \mathbf{d}_{\mathbf{p}(t)} \mathbf{E}_{\text{XUV}}(t - \Delta t) e^{i(\mathbf{v}^2/2 + I_p)t}, \quad (12.22)$$

$$\phi(t) = - \int_t^{+\infty} dt' [\mathbf{v} \mathbf{A}_L(t') + \mathbf{A}_L^2(t')/2]. \quad (12.23)$$

Here,  $\mathbf{E}_{\text{XUV}}(t)$  is the XUV electric field,  $\mathbf{A}_L(t)$  the laser vector potential of the dressing pulse,  $\mathbf{p}(t) = \mathbf{p} + \mathbf{A}(t)$ ,  $\mathbf{d}_{\mathbf{p}}$  the dipole matrix element from the ground state to a continuum state  $|\mathbf{p}\rangle$ ,  $I_p$  the atom's ionization potential.  $\phi(t)$  represents the quantum phase acquired by the electron in the continuum due to its interaction with the laser field. The measured spectrograms are then given by the square modulus of the transition amplitude, i.e.,  $S(\mathbf{v}, \Delta t) = |a(\mathbf{v}, \Delta t)|^2$ .

# FROG-CRAB

Frequency-Resolved Optical Gating for Complete Retrieval of Attosecond Bursts  
Y. Mairesse and F. Quéré, Phys. Rev. A 71, 011401 (2005)

As shown in [69, 70], Eq. (12.23) has an intuitive interpretation: the laser electric field induces a phase modulation on the electron wavepacket during its propagation in the continuum, after being created by the XUV field. In RABBITT, for attosecond XUV pulse trains generated from multi-cycle laser fields, the weak dressing field acts as a periodic phase modulator on the electron wavepacket, thus creating the sidebands that are used to retrieve the harmonic phases. In attosecond streaking, for isolated XUV pulses generated from few-cycle laser fields, the XUV pulse is significantly shorter than then the optical period of the strong streaking laser field, thus creating the characteristic streaking spectrograms.

# FROG-CRAB

Frequency-Resolved Optical Gating for Complete Retrieval of Attosecond Bursts  
Y. Mairesse and F. Quéré, Phys. Rev. A 71, 011401 (2005)

The spectrograms  $S(\mathbf{v}, \Delta t) = |a(\mathbf{v}, \Delta t)|^2$  given by Eq. (12.23) resemble the well-known FROG trace

$$S(\omega, \Delta t) = \left| \int_{-\infty}^{+\infty} dt G(t) E(t - \Delta t) e^{i\omega t} \right|^2 \quad (12.24)$$

In standard FROG,  $G(t)$  represents a pure amplitude gate, and efficient algorithms (e.g., the generalized projections algorithms) can be used to retrieve  $E(t)$  and the gate  $G(t)$  from the spectrogram. Inspection of Eq. (12.23) suggests that in FROG-CRAB,  $G(t) = e^{i\phi(t)}$  could be used as a pure phase gate for the reconstruction. However, a requirement for the applicability of generalized projections algorithms to FROG-CRAB is that there cannot be inseparable terms inside the integrand of Eq. (12.23) that depend both on momentum and time [71]. Obviously, two terms in Eq. (12.23) cause trouble:  $\mathbf{d}_{\mathbf{p}(t)}$  and  $\phi(t)$ . The standard remedy to fix this issue is to make the central momentum approximation (CMA), by substituting  $\mathbf{p}(t)$  with the central momentum of the

# FROG-CRAB

Frequency-Resolved Optical Gating for Complete Retrieval of Attosecond Bursts  
Y. Mairesse and F. Quéré, Phys. Rev. A 71, 011401 (2005)

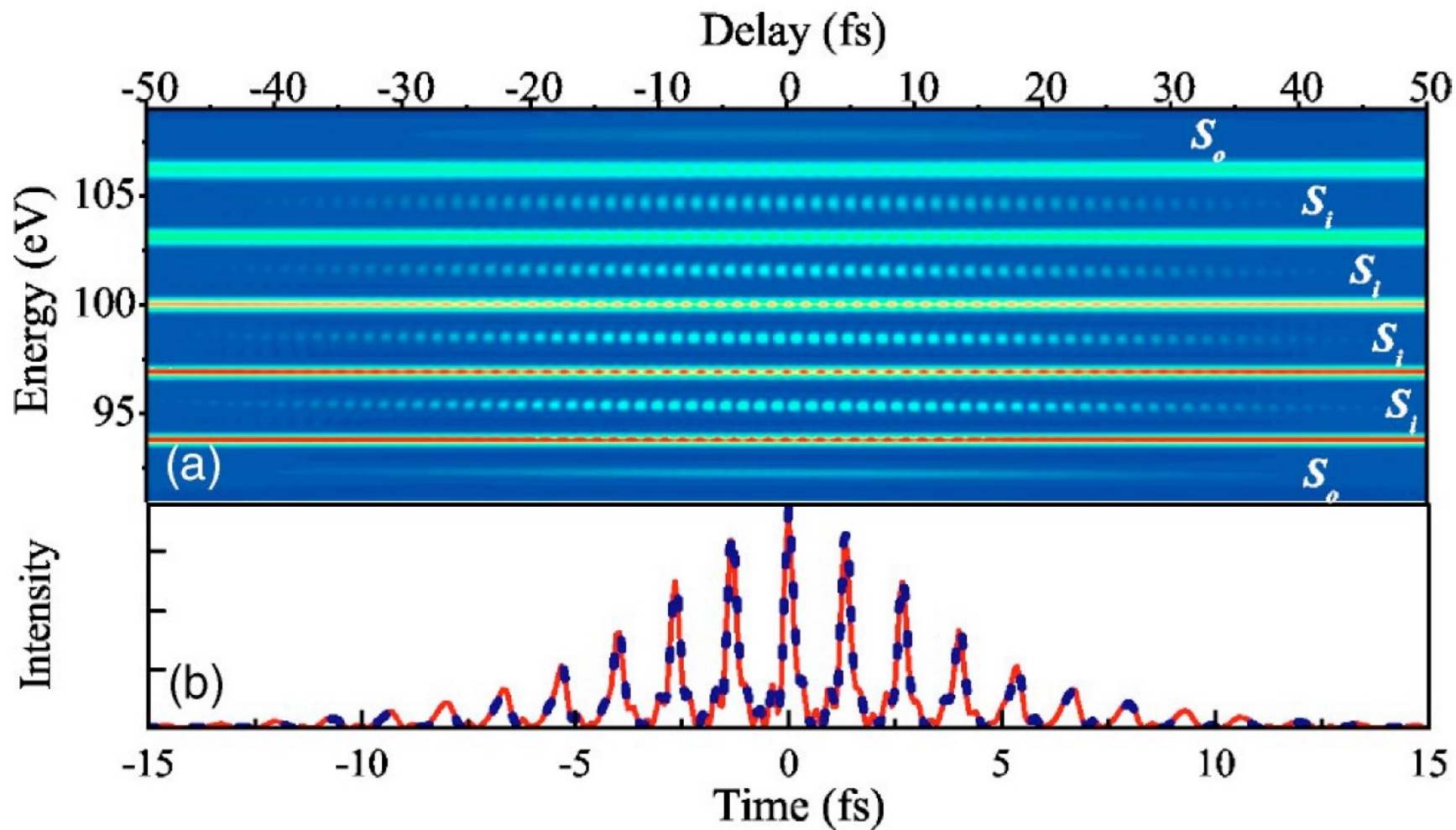
unstreaked electrons  $\mathbf{p}_0$  (and  $\mathbf{v}$  by  $\mathbf{v}_0$ ). The CMA is good as long as the bandwidth of the attosecond pulse is much smaller than the central energy of the photoelectrons. Interestingly, for recent state-of-the-art experiments [19, 20], the CMA is only barely met, the isolated 65-as pulses in [61] already violate this approximation. For such ultrabroadband XUV pulses novel retrieval algorithms, that do not employ the CMA, have been developed, e.g. Phase Retrieval by Omega Oscillation Filtering (PROOF) [72] and Volkov transform generalized projections algorithm (VTGPA) [73].

Coming back to FROG-CRAB: as can be seen by the reconstructions shown in Figs. 12.29, 12.30, and 12.31, FROG-CRAB provides a unified framework to characterize APTs and IAPs and even more complex fields.

PROOF: M. Chini *et al.*, Opt. Express 18, 13006 (2010)

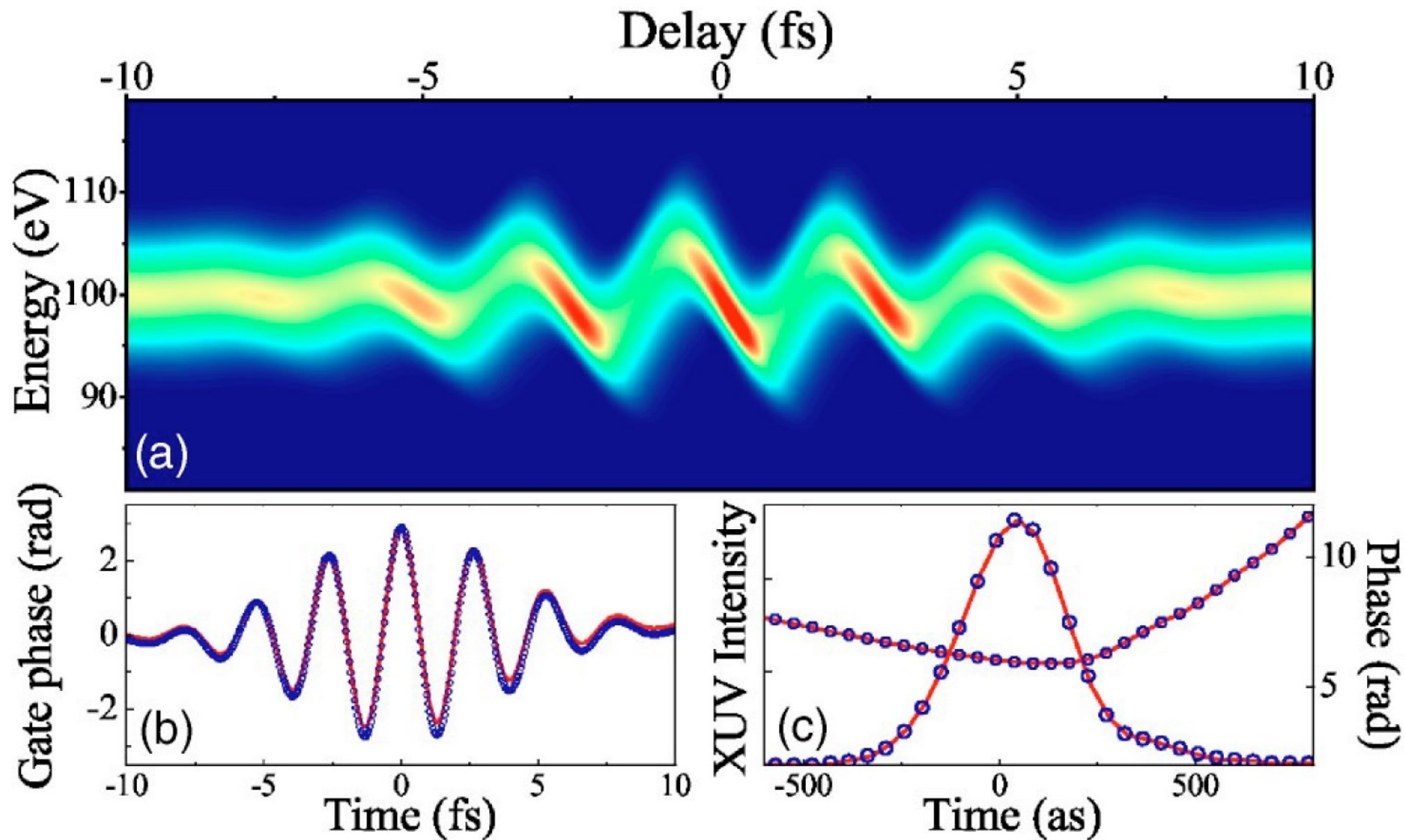
VTGPA: P. D. Keathley *et al.*, New J. Phys. **18**, 073009 (2016)

# FROG-CRAB



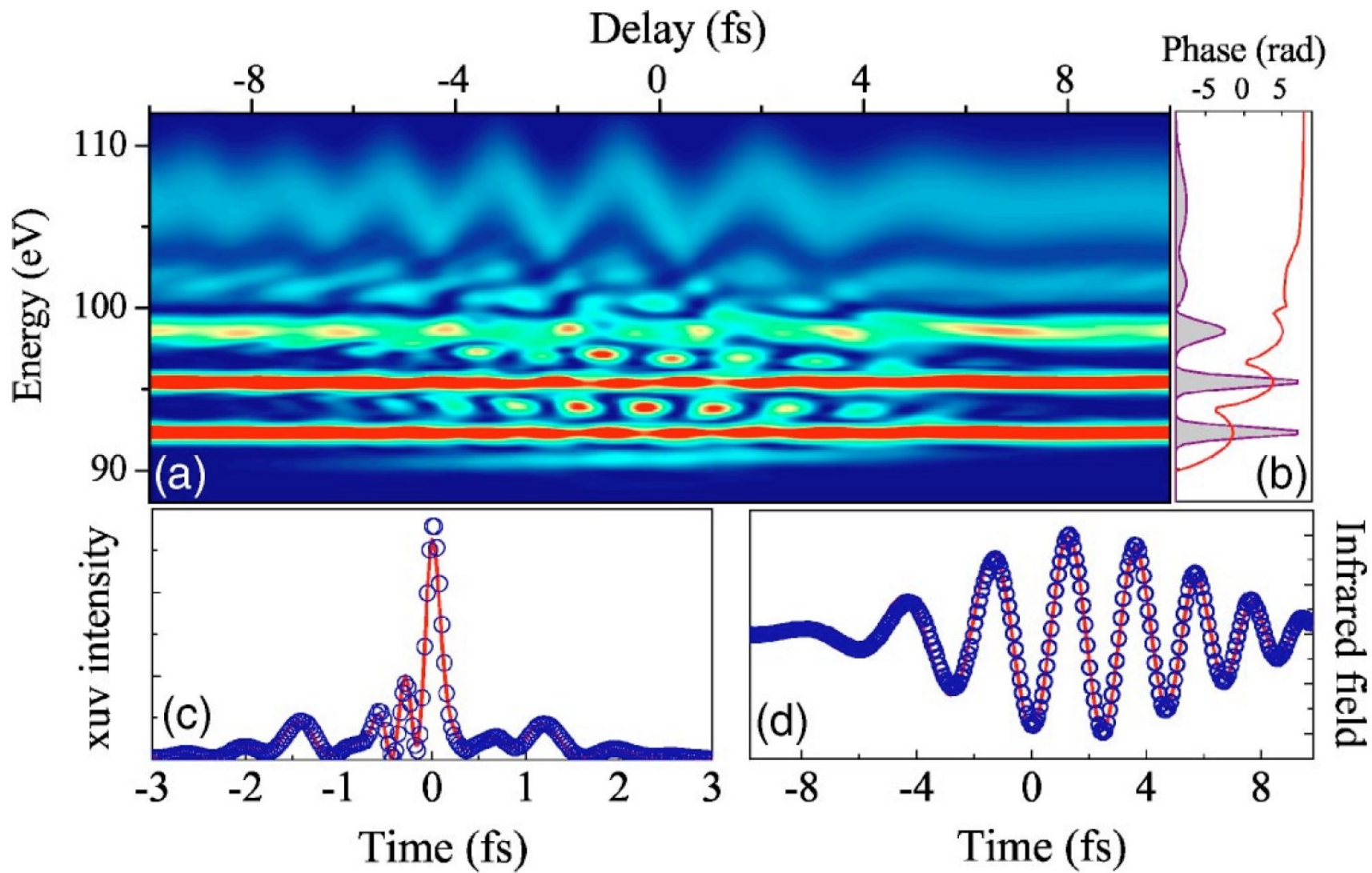
Y. Mairesse and F. Quéré, Phys. Rev. A 71, 011401 (2005)

# FROG-CRAB



Y. Mairesse and F. Quéré, Phys. Rev. A 71, 011401 (2005)

# FROG-CRAB



Y. Mairesse and F. Quéré, Phys. Rev. A 71, 011401 (2005)

## 12.3.7 Transient XUV absorption spectroscopy

changes induced by a first strong pump pulse are probed by the **transient absorption changes of an isolated attosecond XUV pulse**

real-time observation of valence electron motion in Kr:  
E. Goulielmakis *et al.*, Nature **466**, 739 (2010)

observation of Autler-Townes splitting and sub-cycle AC Stark shifts in He:  
M. Chini *et al.*, Sci. Rep. **3**, 1105 (2013).

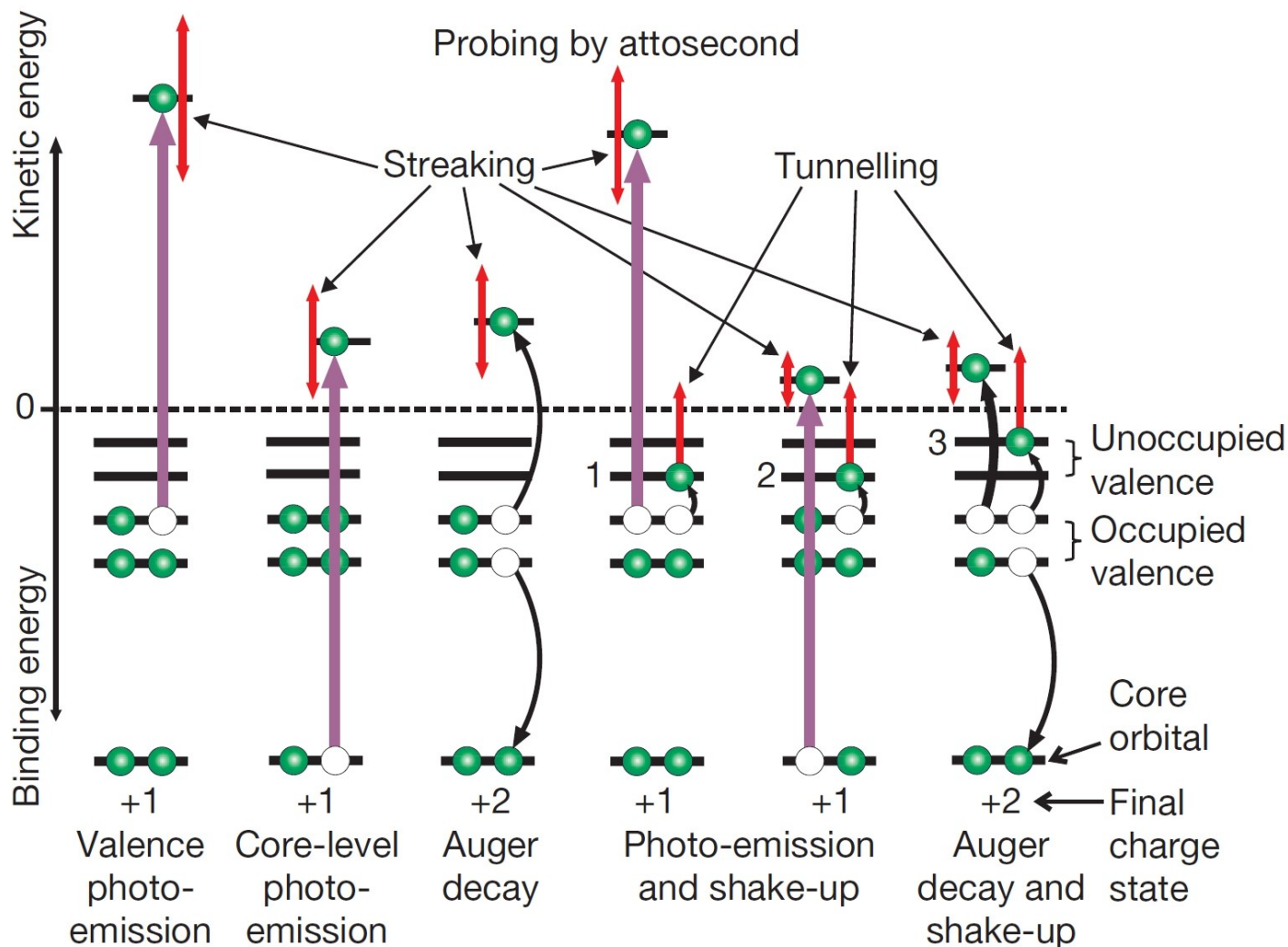
laser control between symmetric Lorentzian and asymmetric Fano line shapes in He:  
C. Ott *et al.*, Science **340**, 716 (2013)

observation and control of two-electron wave packets in He:  
C. Ott *et al.*, Nature **516**, 374 (2014)

**Show video!**

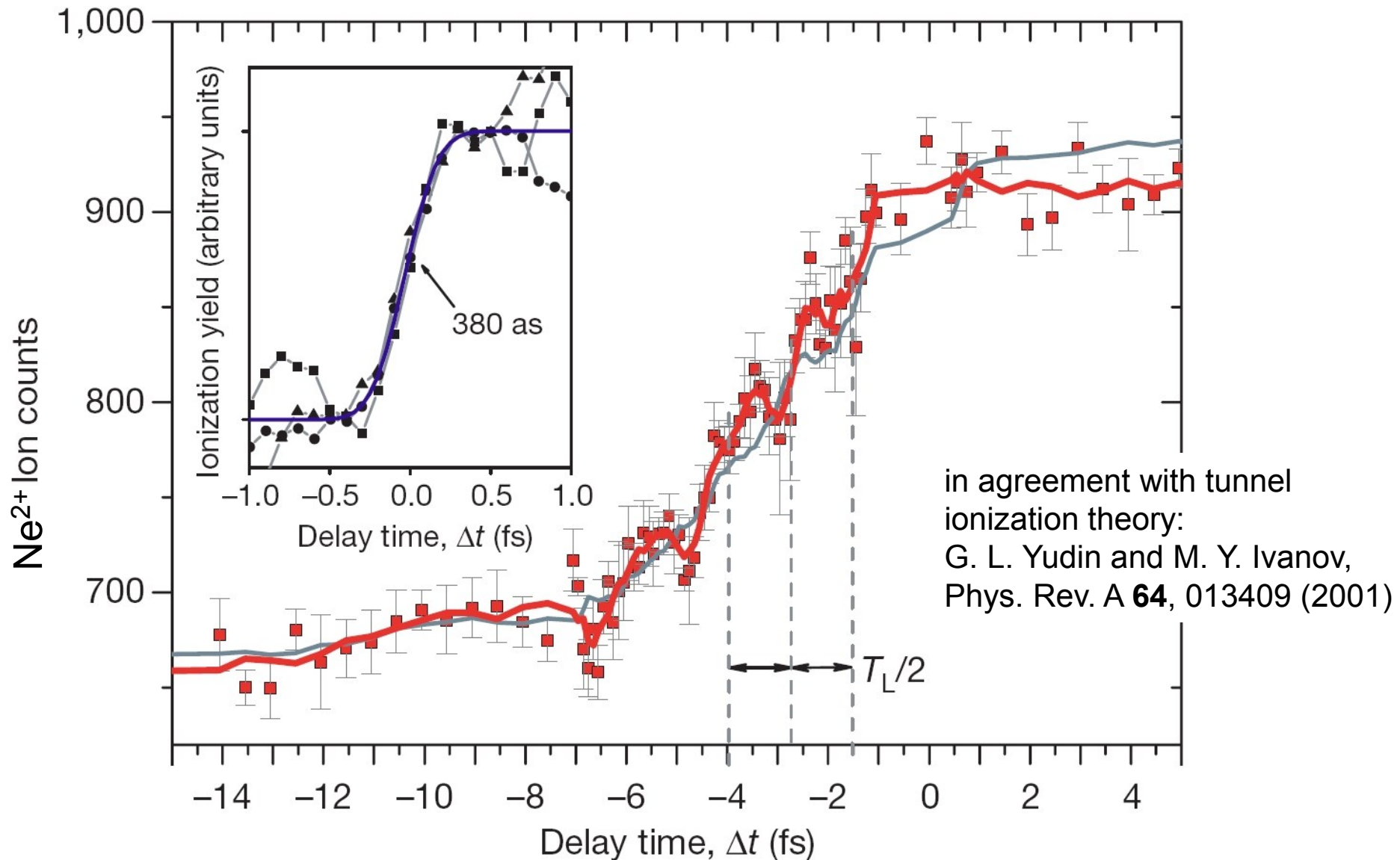
# 12.3.8 Attosecond ion-charge-state chronoscopy

attosecond tunneling spectroscopy



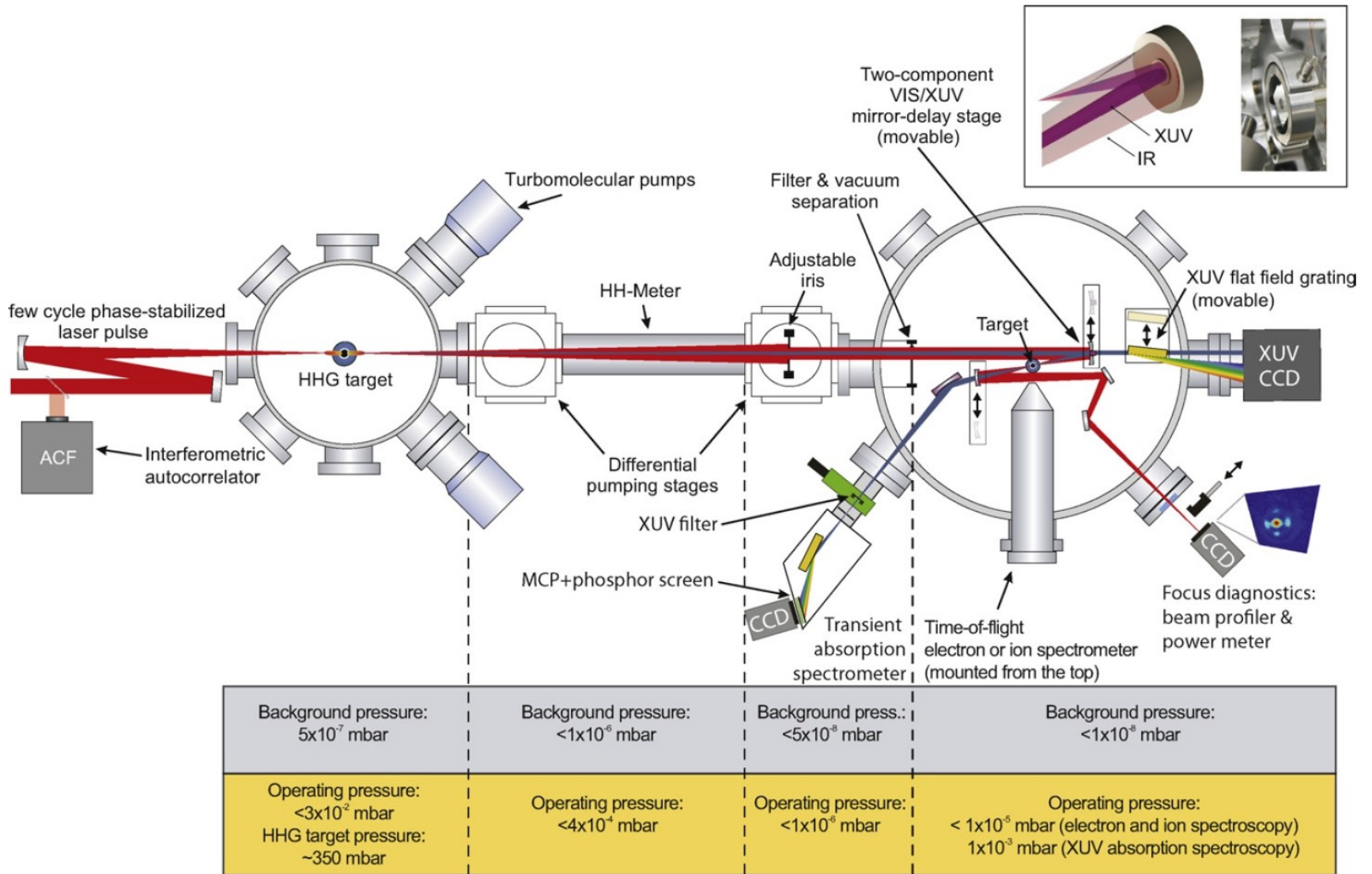
M. Uiberacker *et al.*, Nature **446**, 627 (2007)

# Attosecond tunneling spectroscopy

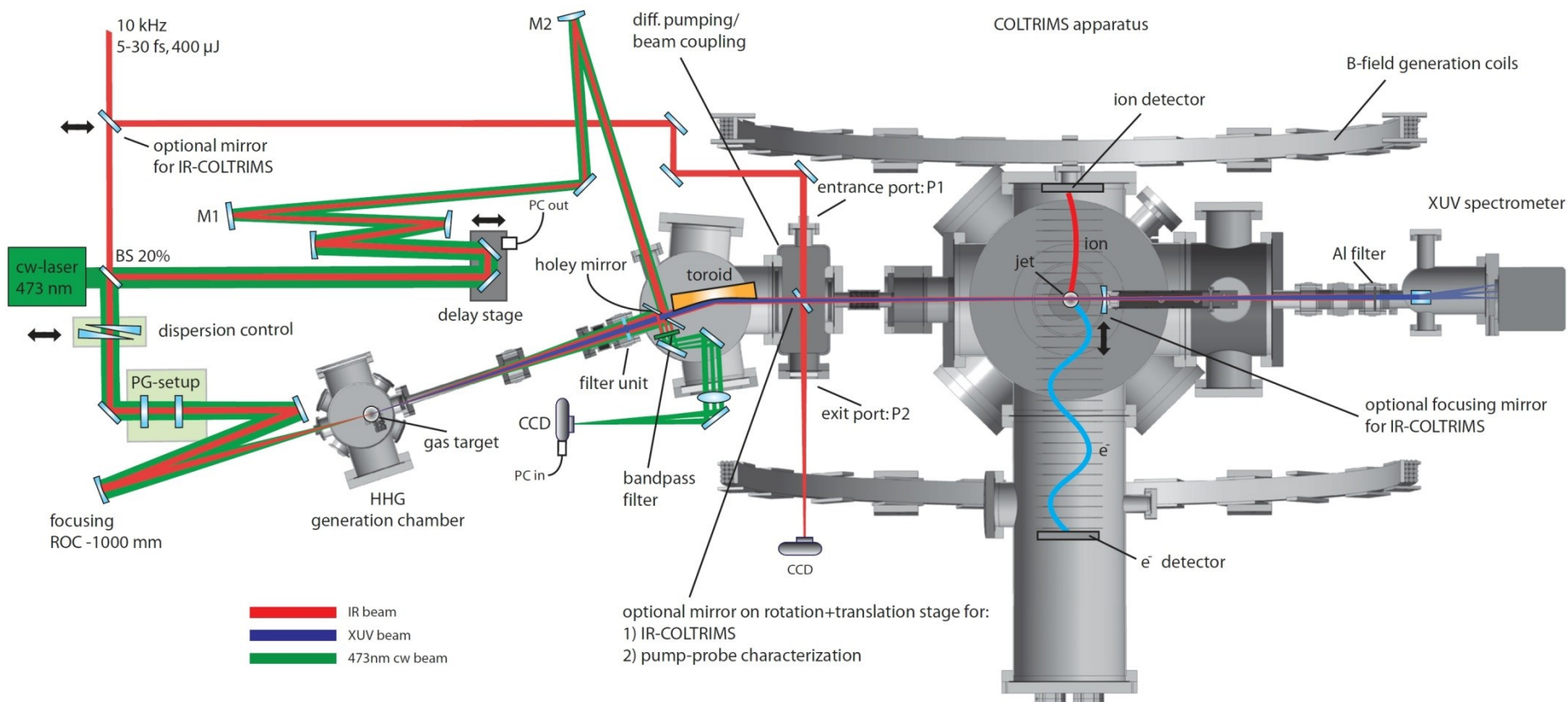


M. Uiberacker *et al.*, Nature **446**, 627 (2007)

# 12.3.9 Attoscience beamline at MPQ Garching



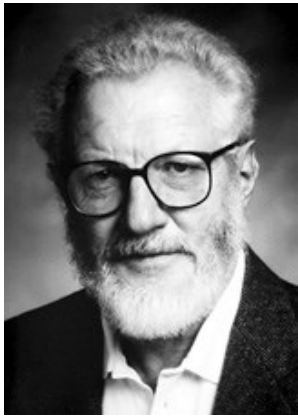
# 12.3.9 Attoscience beamline at ETH Zürich



# Chapter 13: Strong-field physics in solids

strong-field (i.e., nonperturbative) phenomena in solids

many physical processes currently of interest in this research area already known for decades, but only thanks to the advent of modern state-of-the-art intense few-cycle pulses, in particular in mid-IR or THz, they can now experimentally be investigated



Herbert Kroemer's Nobel Prize autobiography (2000):  
"... it became obvious that the huge fields required for **Bloch oscillations in a bulk semiconductor** could never be reached."

In addition, rapid progress in the field of **quantum materials**

D. N. Basov, R. D. Averitt, and D. Hsieh, *Nature Materials* **81**, 1077 (2017)

# 13.1 examples: semiconductors GaAs and ZnO

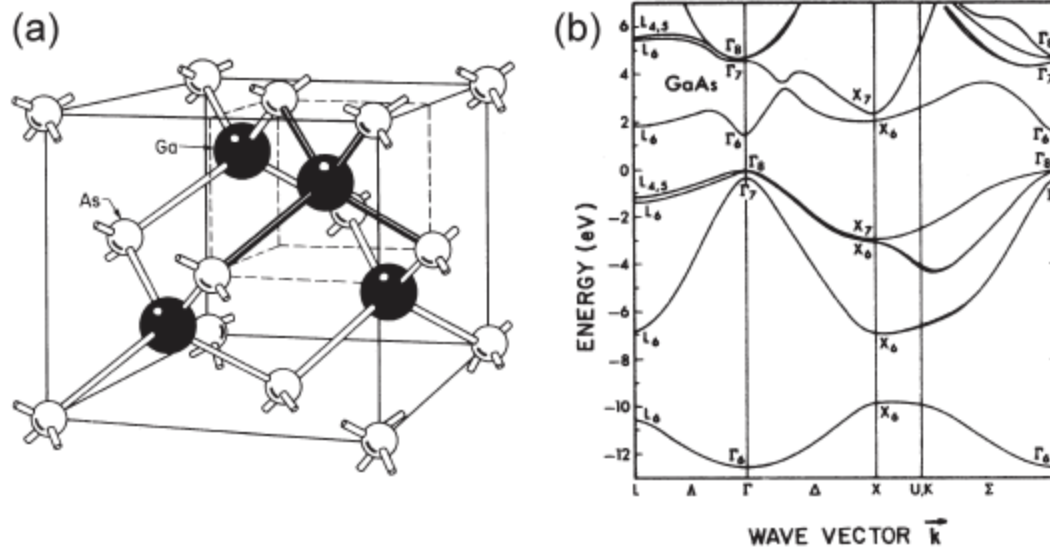


Figure 13.1: (a) Zinc blende structure of GaAs [6]. (b) Band structure of GaAs [7].

III-V direct gap semiconductor, **1.42 eV band gap**

no inversion symmetry

detailed discussion of band structure in Lecture Notes pages 308-309

# 13.1 examples: semiconductors GaAs and ZnO

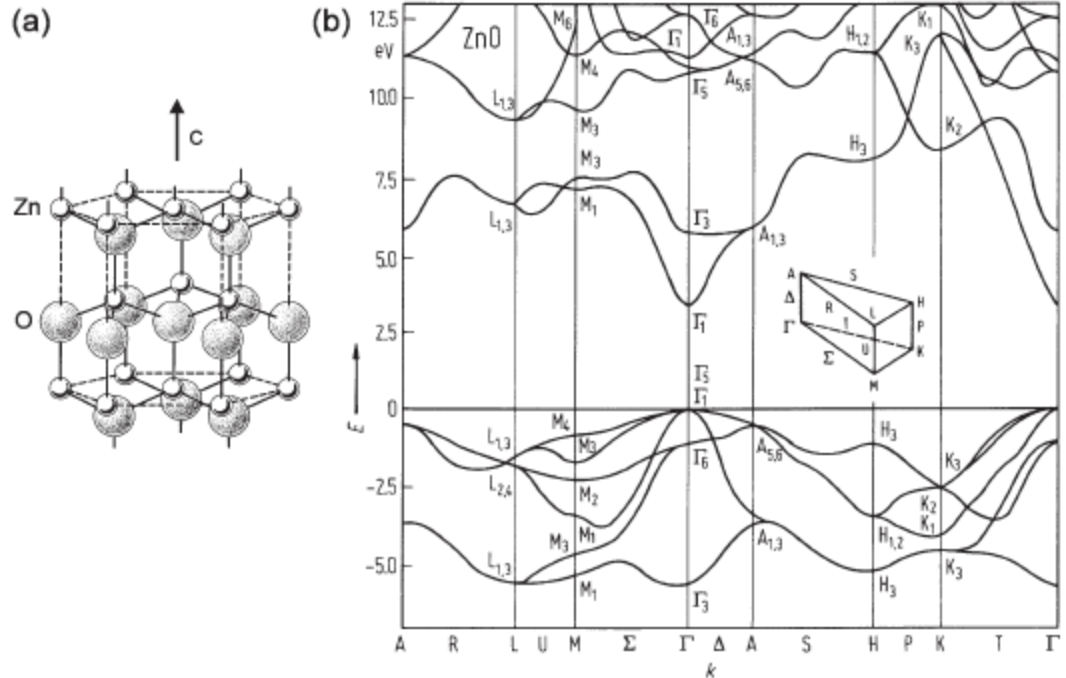


Figure 13.2: (a) Wurtzite structure of ZnO, the crystallographic  $\vec{c}$ -axis is indicated [9]. (b) Band structure of ZnO [10]. In this band-structure calculation, spin-orbit interaction was not included. The inset illustrates the points and directions of high symmetry of the Brillouin zone.

II-VI direct gap semiconductor, **3.3 eV band gap**

ZnO has a  $\vec{c}$ -axis without inversion symmetry and it is birefringent (electric field  $\vec{E} \parallel \vec{c}$  and  $\vec{E} \perp \vec{c}$  are inequivalent).

detailed discussion of band structure in Lecture Notes pages 309-310

# Extreme nonlinear optics in solids, atoms, molecules

ponderomotive energy  $U_p \propto \lambda^2 I / m_e$

## semiconductors

resonant effects (GaAs:  $\Omega / \omega_0 = 1$ )

off-resonant effects (ZnO:  $\Omega / \omega_0 = 2.2$ )

electron mass  $m_e$

$0.067 \times m_0$

$0.24 \times m_0$

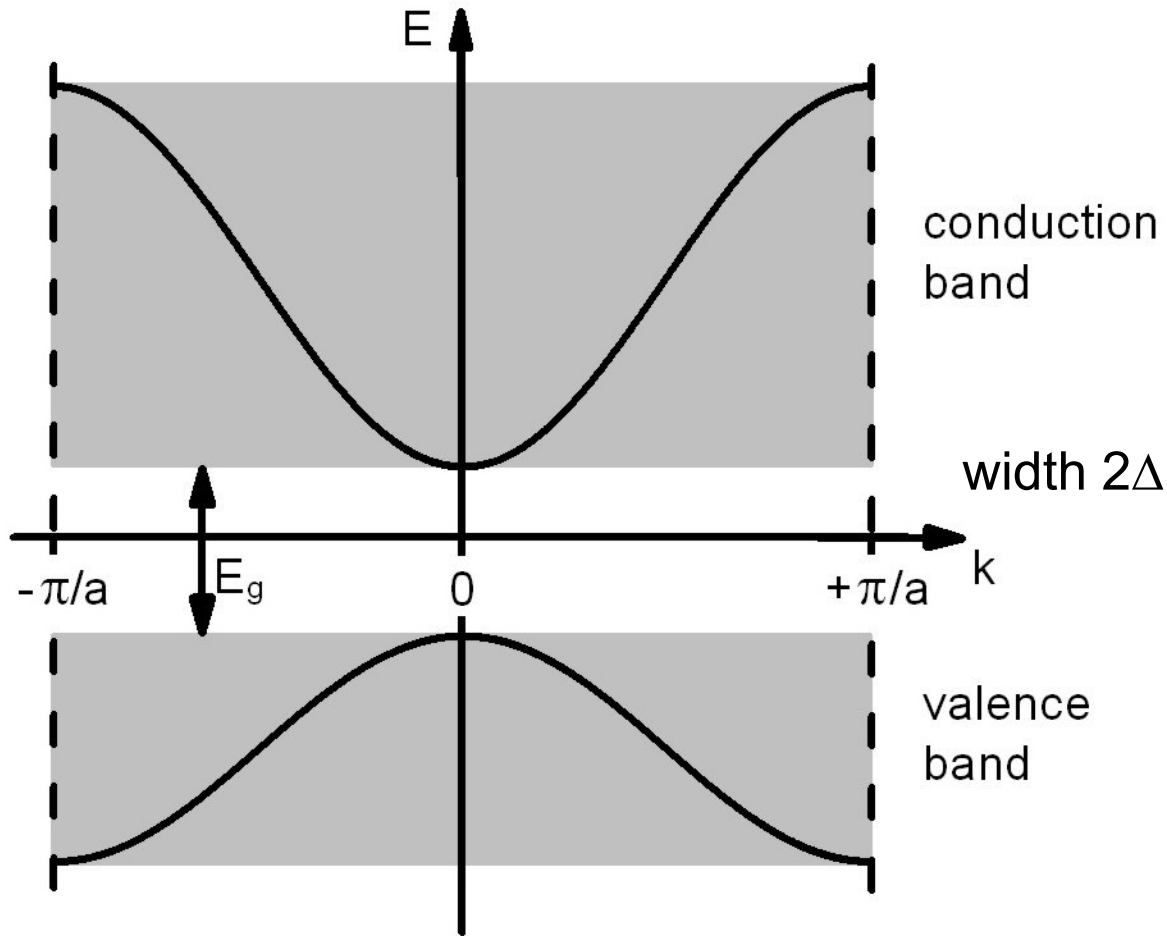
## atoms and molecules

far off-resonant effects (Neon:  $I_p / \hbar$  )  $m_0$

→ required intensities 2-3 orders of magnitude larger than in semiconductors!

strong-field excitation with UV – VIS – IR – THz driver pulses, very different from gas case which is typically far off-resonant

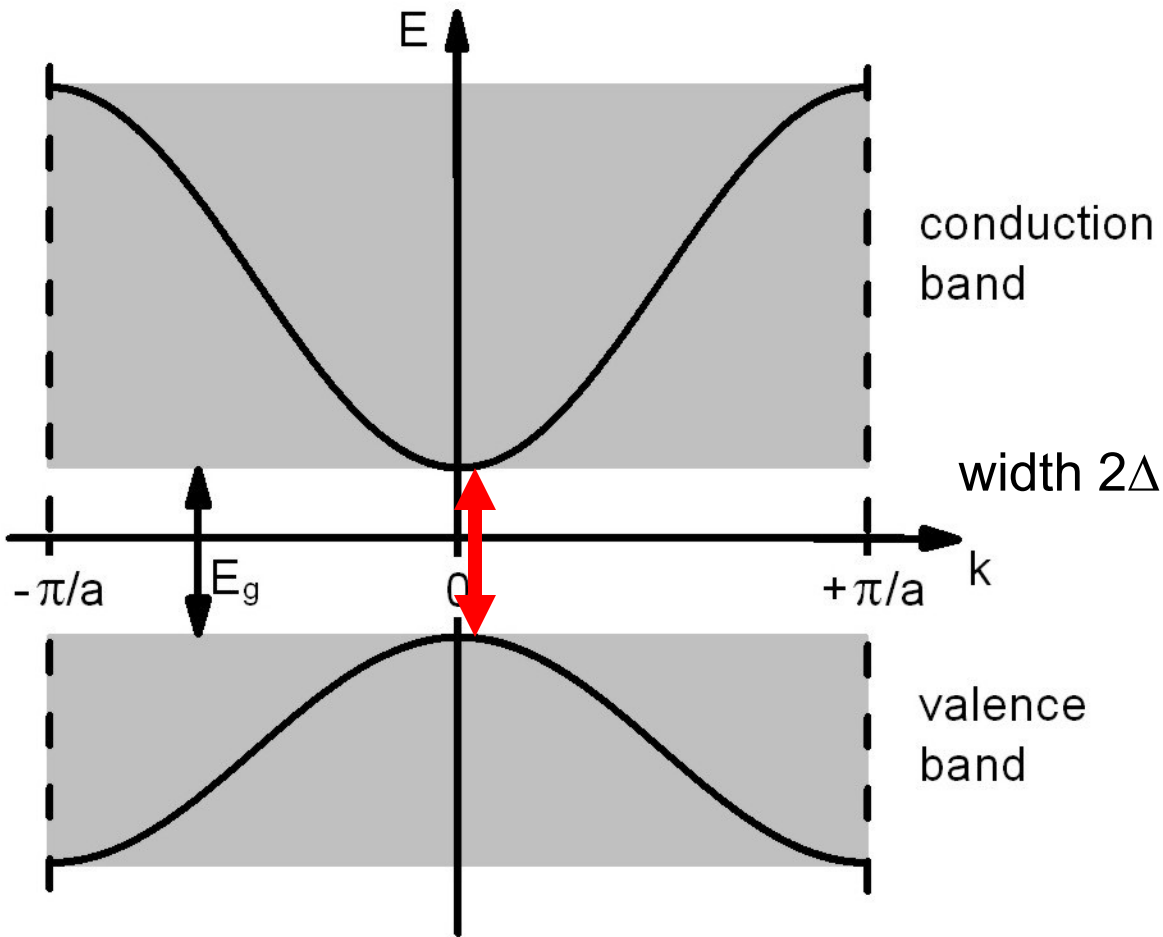
## 13.2 Energy scales of strong-field interactions in solids



O. D. Mücke *et al.*, in *Topics Appl. Phys.* **95**, 379  
(Springer, Berlin, 2004)

M. Wegener, *Extreme Nonlinear Optics*  
(Springer, Berlin, 2005)

# 13.2 Energy scales of strong-field interactions in solids



interband transitions

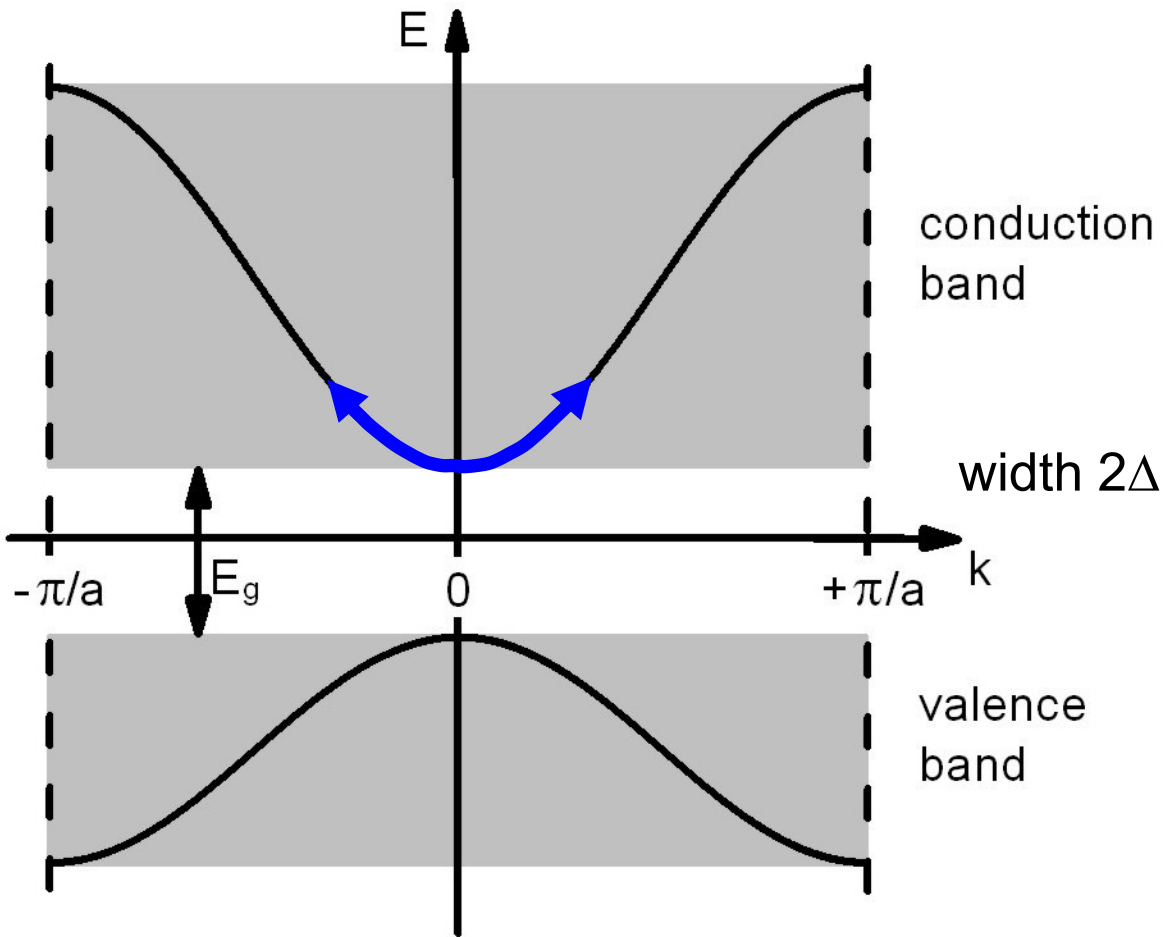
Rabi energy

$$\hbar \Omega_R \approx \int dE$$

optical Bloch equations

O. D. Mücke *et al.*, in *Topics Appl. Phys.* **95**, 379  
 (Springer, Berlin, 2004)  
 M. Wegener, *Extreme Nonlinear Optics*  
 (Springer, Berlin, 2005)

# 13.2 Energy scales of strong-field interactions in solids



**interband transitions**

**Rabi energy**

$$\hbar \Omega_R = \int dE$$

**intraband transitions**

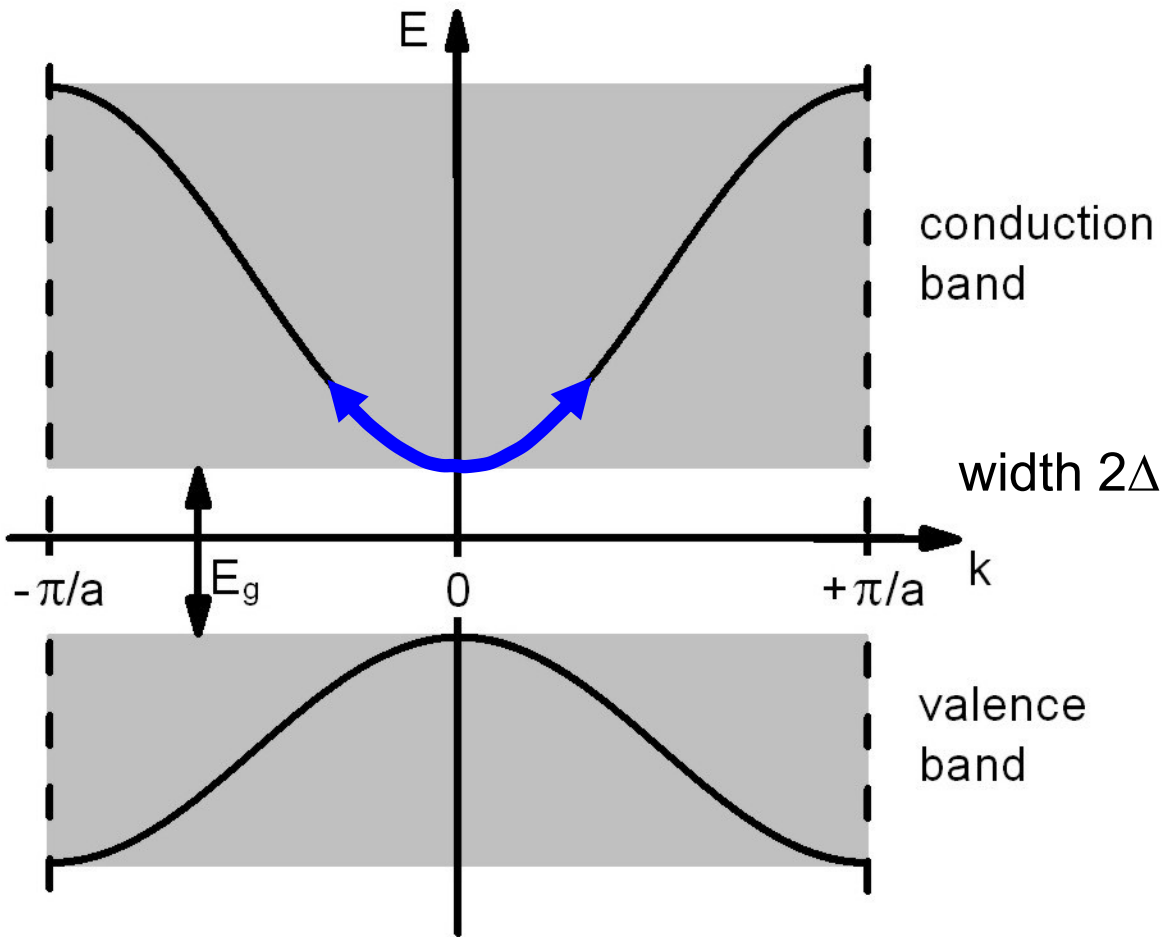
**ponderomotive energy**

$$U_p = \frac{e^2 E^2}{4m_e \omega^2}$$

(limited validity within effective mass approximation!)

O. D. Mücke *et al.*, in *Topics Appl. Phys.* **95**, 379 (Springer, Berlin, 2004)  
 M. Wegener, *Extreme Nonlinear Optics* (Springer, Berlin, 2005)

# 13.2 Energy scales of strong-field interactions in solids



**interband transitions**

**Rabi energy**

$$\hbar \Omega_R \propto \int dE$$

**intraband transitions**

**ponderomotive energy**

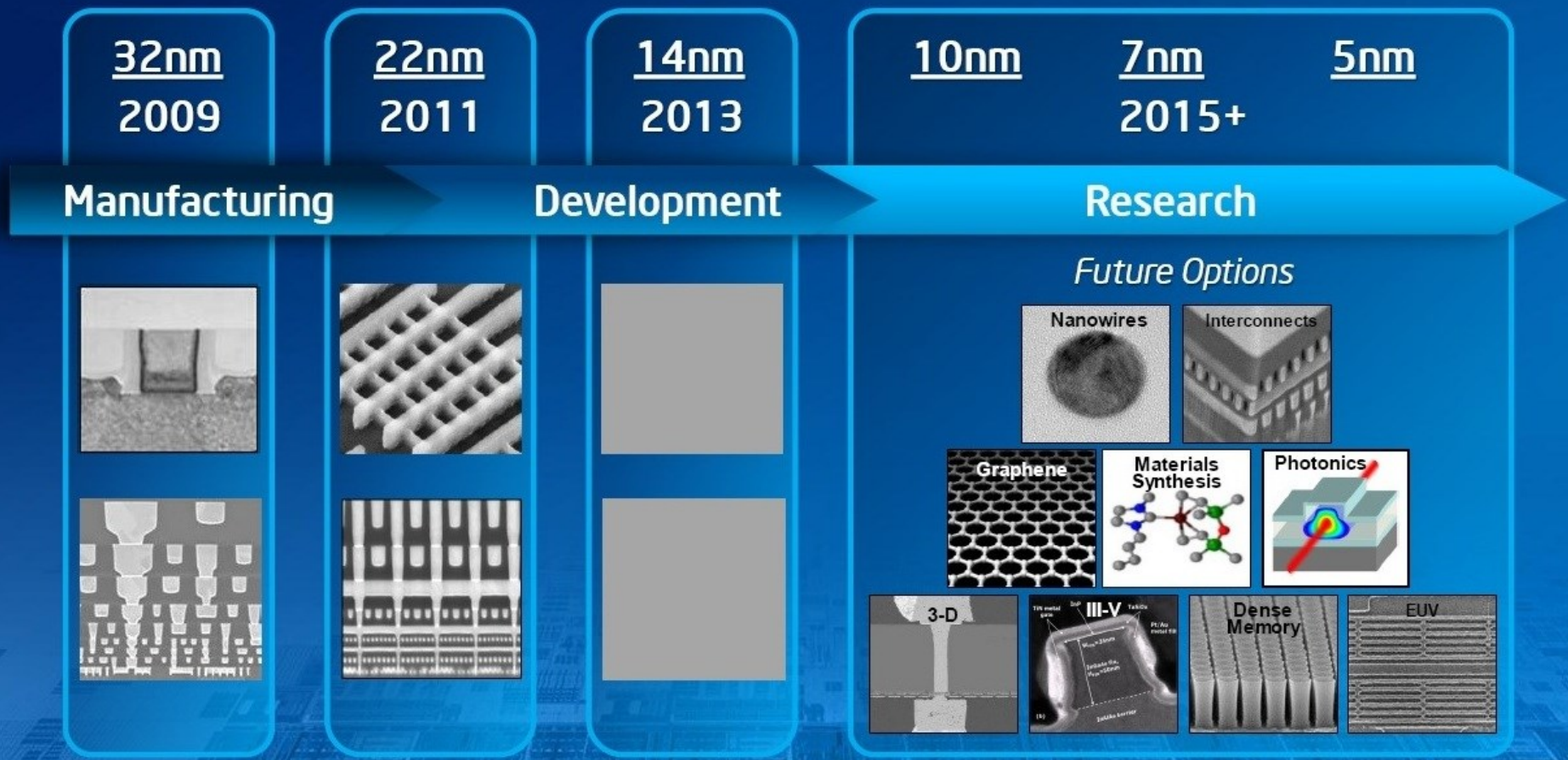
$$U_p = \frac{e^2 E^2}{4m_e \omega^2}$$

(limited validity within effective mass approximation!)

**Bloch energy**

$$\hbar \Omega_B \propto a e E$$

O. D. Mücke *et al.*, in *Topics Appl. Phys.* **95**, 379 (Springer, Berlin, 2004)  
 M. Wegener, *Extreme Nonlinear Optics* (Springer, Berlin, 2005)



Source: Intel

Future options subject to change

**ever decreasing gate length** (14nm in 2013, potentially 5nm in 2015+)

- higher potential drops in semiconductor structures
- extremely strong electric fields ( $\sim 1$  V/nm)
- energy scales of strong-field interactions (ponderomotive, Rabi, Bloch energies) become comparable to characteristic energies of semiconductor ( $\sim 1$  eV)

**extreme light-matter interactions** (underlying physics, feasibility of scaling...)

## 13.3 Semiconductor Bloch equations

interacting **electrons and holes within a strongly excited solid** have to be treated as a **system far from equilibrium**

**semiconductor Bloch equations** treat the Coulomb interaction consistently on a **Hartree-Fock level**, and include many-body and phase space effects such as, **e.g., band-gap renormalization, Pauli blocking, and screening**

Hamiltonian (in second quantization, no intraband driving)

$$\begin{aligned} H = & \sum_{\vec{k}} E_c(\vec{k}) c_{c\vec{k}}^\dagger c_{c\vec{k}} + \sum_{\vec{k}} E_v(\vec{k}) c_{v\vec{k}}^\dagger c_{v\vec{k}} \\ & + \frac{1}{2} \sum_{\vec{k}, \vec{k}', \vec{q} \neq 0} v(\vec{q}) \left[ c_{c, \vec{k} + \vec{q}}^\dagger c_{c, \vec{k}' - \vec{q}}^\dagger c_{c\vec{k}'} c_{c\vec{k}} + c_{v, \vec{k} + \vec{q}}^\dagger c_{v, \vec{k}' - \vec{q}}^\dagger c_{v\vec{k}'} c_{v\vec{k}} + 2c_{c, \vec{k} + \vec{q}}^\dagger c_{v, \vec{k}' - \vec{q}}^\dagger c_{v\vec{k}'} c_{c\vec{k}} \right] \\ & - E(\vec{r}, t) \sum_{\vec{k}} \left[ d_{cv}(\vec{k}) c_{c\vec{k}}^\dagger c_{v\vec{k}} + \text{h.c.} \right]. \end{aligned} \quad (13.21)$$

The equation of motion of the optical transition amplitudes

$$p_{vc}(\vec{k}) = \langle c_{v\vec{k}}^\dagger c_{c\vec{k}} \rangle \quad (13.22)$$

(depending on time  $t$  as well as parametrically on the spatial coordinate  $\vec{r}$ ) and those of the occupation numbers in the conduction band

$$f_c(\vec{k}) = \langle c_{c\vec{k}}^\dagger c_{c\vec{k}} \rangle \quad (13.23)$$

and in the valence band

$$f_v(\vec{k}) = \langle c_{v\vec{k}}^\dagger c_{v\vec{k}} \rangle \quad (13.24)$$

are easily calculated from the Heisenberg equation of motion for an arbitrary operator  $\mathcal{O}$  according to

$$-i\hbar \frac{\partial}{\partial t} \mathcal{O} = [H, \mathcal{O}], \quad (13.25)$$

while employing the usual fermionic anticommutation relations, i.e.,

$$[c_{c\vec{k}}, c_{c\vec{k}'}^\dagger]_+ = \delta_{\vec{k}\vec{k}'}, \quad [c_{v\vec{k}}, c_{v\vec{k}'}^\dagger]_+ = \delta_{\vec{k}\vec{k}'}, \quad (13.26)$$

and that all other anticommutators are zero. The resulting equations of motions include couplings to higher-order correlations. With the help of a quantum-mechanical projection-operator technique it was shown in Ref. [38], that (without approximation) the density matrix can be projected into a "coherent contribution" and a "scattering contribution", respectively, and that the time evolution of an arbitrary operator  $\mathcal{O}$  is governed by

$$\frac{\partial}{\partial t} \langle \mathcal{O} \rangle = \frac{\partial}{\partial t} \langle \mathcal{O} \rangle_{\text{coh}} + \frac{\partial}{\partial t} \langle \mathcal{O} \rangle_{\text{scat}}. \quad (13.27)$$

After some lengthy but straightforward operator algebra this leads to the semiconductor Bloch equations for the transition amplitude

$$\left( \frac{\partial}{\partial t} + i\hbar^{-1} \left[ \hat{E}_c(\vec{k}) - \hat{E}_v(\vec{k}) \right] \right) p_{vc}(\vec{k}) + \left( \frac{\partial}{\partial t} p_{vc}(\vec{k}) \right)_{\text{scat}} = i\hat{\Omega}_R(\vec{r}, \vec{k}, t) \left[ f_v(\vec{k}) - f_c(\vec{k}) \right], \quad (13.28)$$

for the distribution function of the conduction band

$$\frac{\partial}{\partial t} f_c(\vec{k}) + \left( \frac{\partial}{\partial t} f_c(\vec{k}) \right)_{\text{scat}} = -2\text{Im} \left( \hat{\Omega}_R(\vec{r}, \vec{k}, t) p_{vc}^*(\vec{k}) \right), \quad (13.29)$$

and a corresponding equation for the distribution function of the valence band. The terms with subscript "scat" describe dephasing and relaxation originating from many-body interactions beyond the Hartree-Fock level. As we will see later, on a time scale close to an optical cycle, these terms can become appreciable under extreme excitation conditions.

Within the framework of the semiconductor Bloch equations, the Coulomb interaction leads to a renormalization<sup>5</sup> of the energies according to

$$\hat{E}_c(\vec{k}) = E_c(\vec{k}) - \sum_{\vec{k}'} v(\vec{k} - \vec{k}') f_c(\vec{k}') \quad (13.30)$$

$$\hat{E}_v(\vec{k}) = E_v(\vec{k}) + \sum_{\vec{k}'} v(\vec{k} - \vec{k}') f_v(\vec{k}') \quad (13.31)$$

as well as to a renormalized Rabi energy

$$\hbar\hat{\Omega}_R(\vec{r}, \vec{k}, t) = d_{cv}(\vec{k})E(\vec{r}, t) + \sum_{\vec{k}'} v(\vec{k} - \vec{k}') p_{vc}(\vec{k}'). \quad (13.32)$$

Thus, the carriers do not react to the applied laser field  $E(\vec{r}, t)$  alone, but to the applied laser field plus the "internal" field which is the sum over interband transition amplitudes  $p_{vc}$  times the Coulomb interaction  $v$ . Furthermore, the renormalization terms lead to a coupling of different  $\vec{k}$  states.

The *optical polarization*, which enters the Maxwell equations, is given by

$$P(\vec{r}, t) = \sum_{\vec{k}} d_{cv}(\vec{k}) \left( p_{vc}(\vec{k}) + \text{c.c.} \right) + P_b(\vec{r}, t), \quad (13.33)$$

Sometimes, a background polarization  $P_b(\vec{r}, t) = \varepsilon_0 \chi_b(\vec{r}) E(\vec{r}, t) = \varepsilon_0 (\varepsilon_b(\vec{r}) - 1) E(\vec{r}, t)$  is employed, which approximately accounts for all "very" high-energy optical transitions not explicitly accounted for in the underlying Hamiltonian. It can be expressed in terms of the background dielectric constant  $\varepsilon_b(\vec{r})$ .

Now, including additional terms in the Hamiltonian (13.21), that also take into account intraband driving

$$H_{\text{intra}} = ieE(\vec{r}, t) \sum_{\vec{k}} \left[ c_{c\vec{k}}^\dagger \nabla_{\vec{k}} c_{c\vec{k}} + c_{v\vec{k}}^\dagger \nabla_{\vec{k}} c_{v\vec{k}} + \text{h.c.} \right] \quad (13.35)$$

[but ignoring electron-phonon coupling in this section, since on time scale of the light period (i.e., the relevant scale we are interested in here in this section) electron-phonon coupling is not expected to be important (as typical phonon periods are on the order of  $\sim 100$  fs)], one can derive the semiconductor Bloch equations for the coupled interband and intraband dynamics [42, 43] given by

$$\begin{aligned} & \left( \frac{\partial}{\partial t} + i\hbar^{-1} \left[ \hat{E}_c(\vec{k}) - \hat{E}_v(\vec{k}) \right] \right) p_{vc}(\vec{k}) + \left( \frac{\partial}{\partial t} p_{vc}(\vec{k}) \right)_{\text{scat}} \\ & = i\hat{\Omega}_R(\vec{r}, \vec{k}, t) \left[ f_v(\vec{k}) - f_c(\vec{k}) \right] + e\hbar^{-1} E(\vec{r}, t) \nabla_{\vec{k}} p_{vc}(\vec{k}), \end{aligned} \quad (13.36)$$

and

$$\frac{\partial}{\partial t} f_c(\vec{k}) + \left( \frac{\partial}{\partial t} f_c(\vec{k}) \right)_{\text{scat}} = -2\text{Im} \left( \hat{\Omega}_R(\vec{r}, \vec{k}, t) p_{vc}^*(\vec{k}) \right) + e\hbar^{-1} E(\vec{r}, t) \nabla_{\vec{k}} f_c(\vec{k}), \quad (13.37)$$

plus again a corresponding equation for the distribution function of the valence band. We immediately identify the terms related to interband transitions,  $\hat{\Omega}_R$ , and to intraband transitions,  $E\nabla_{\vec{k}}$ . Beside the optical polarization (13.33), one has an additional source term in Maxwell's equations given by the induced *intraband current*

$$J(\vec{r}, t) = e \sum_{\vec{k}} \left( v_{cg}(\vec{k}) f_c(\vec{k}) + v_{vg}(\vec{k}) f_v(\vec{k}) \right), \quad (13.38)$$

where  $\vec{v}_{ig}(\vec{k}) = \nabla_{\vec{k}} E_i(\vec{k})/\hbar$  denotes the group velocities of the valence and conduction bands ( $i = v, c$ ), respectively. From the Maxwell's equation, it follows that the radiated spectrum is given by

$$I_{\text{rad}}(\omega) \propto |\omega^2 P(\omega) + i\omega J(\omega)|^2 \quad (13.39)$$

It is immediately clear from the semiconductor Bloch equations (13.37)-(13.37) combined with Eq. (13.39), within this theoretical framework interband and intraband transitions are inherently coupled in a nontrivial way, which generally leads to complex coupled dynamics for strong excitations, in particular for the case of high-harmonic generation from solids (see Section 13.6). Thus, it is crucial to realize, that in the general strong-field interaction case, it is *NOT possible* to experimentally isolate either interband or intraband dynamics and study them in an independent, decoupled way.

The dependence of the internal structure of a particle on the dynamical parameter can give rise to anomalous transport properties — in particular, the Berry-phase effect<sup>174</sup>. The Berry phase can be characterized by the Berry curvature,  $\Omega$ , which behaves like an effective magnetic field in momentum space. In the context of Bloch electrons — that is, electrons that occupy a Bloch band of a crystalline solid —  $\Omega$  originates from the dependence of the periodic part of the Bloch function,  $u_{n,\mathbf{k}}$ , on the wave vector  $\mathbf{k}$ . Consider a wave packet of a Bloch electron moving adiabatically in a non-degenerate energy band with band index  $n$ . In many situations, the wave packet has a real-space extension that is much larger than the lattice constant but much smaller than the length scale of the external perturbation; thus, the wave vector and the position of the wave packet can be considered simultaneously. The electron wave packet can then be described by the semiclassical transport equations of motion<sup>14,16</sup>:

$$\dot{\mathbf{r}} = \frac{1}{\hbar} \frac{\partial E_{n,\mathbf{k}}}{\partial \mathbf{k}} - \dot{\mathbf{k}} \times \Omega_{n,\mathbf{k}} \quad \hbar \dot{\mathbf{k}} = -e\mathbf{E} - e\dot{\mathbf{r}} \times \mathbf{B}$$

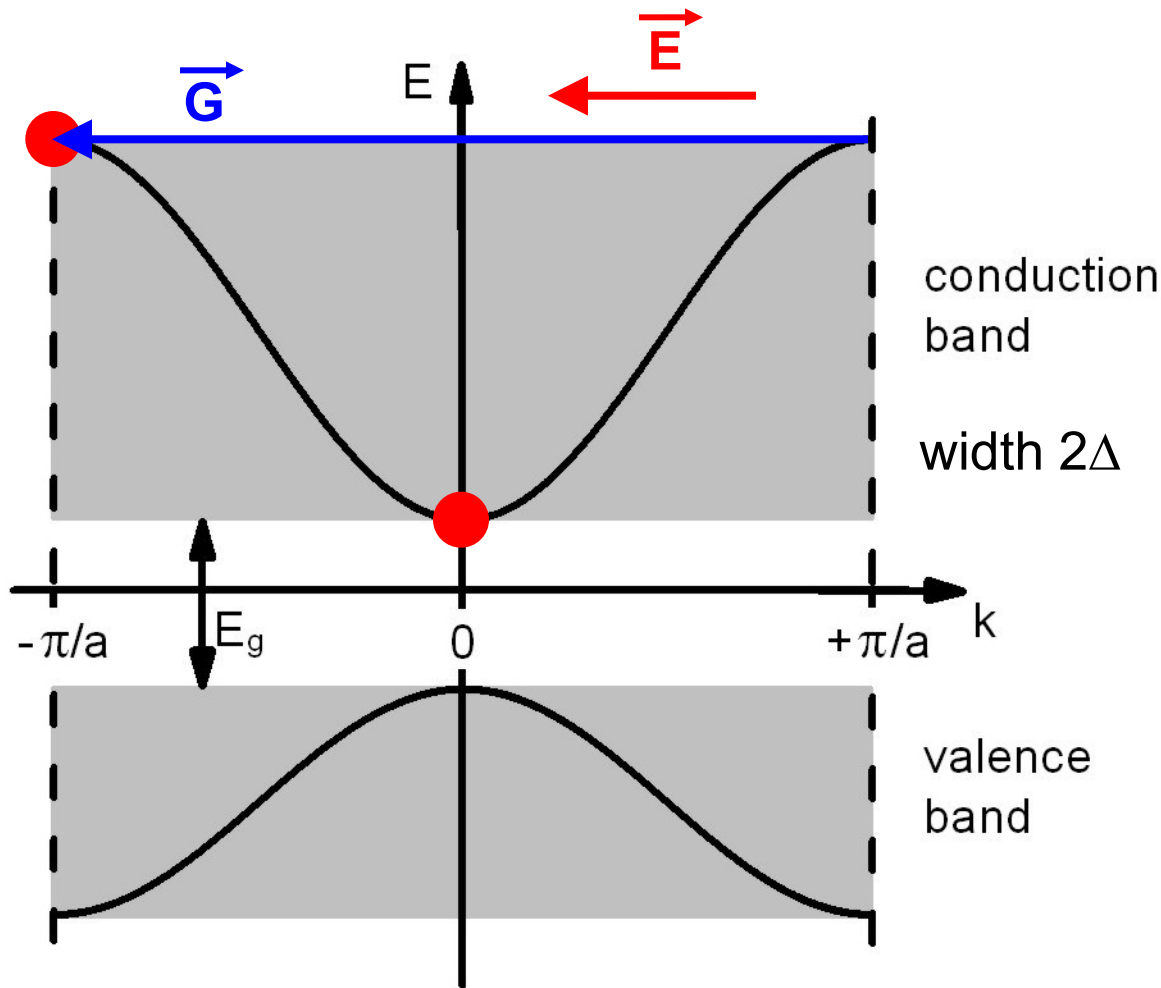
where  $E_{n,\mathbf{k}}$  and  $\Omega_{n,\mathbf{k}}$  are the energy dispersion and Berry curvature of the  $n$ th band,  $\mathbf{k}$  and  $\mathbf{r}$  are the crystal momentum and position of the electron wave packet, and  $\mathbf{E}$  and  $\mathbf{B}$  are the external electric and magnetic field, respectively. The dot represents the first derivative with respect to time. The term  $\dot{\mathbf{k}} \times \Omega_{n,\mathbf{k}}$  gives rise to an anomalous velocity perpendicular to  $\mathbf{E}$  (that is, the Hall effect).

J. R. Schaibley *et al.*, Nature Reviews Materials **1**, 16055 (2016)

D. Xiao, M.-C. Chang, and Q. Niu, Rev. Mod. Phys. **82**, 1959 (2010)

# 13.6 HHG from solids

## Bloch oscillations in bulk solids

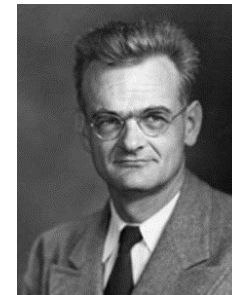


acceleration theorem

$$\vec{F} = \hbar \dot{\vec{k}} = e\vec{E}$$



Felix Bloch,  
Z. Phys. **52**,  
555 (1929)

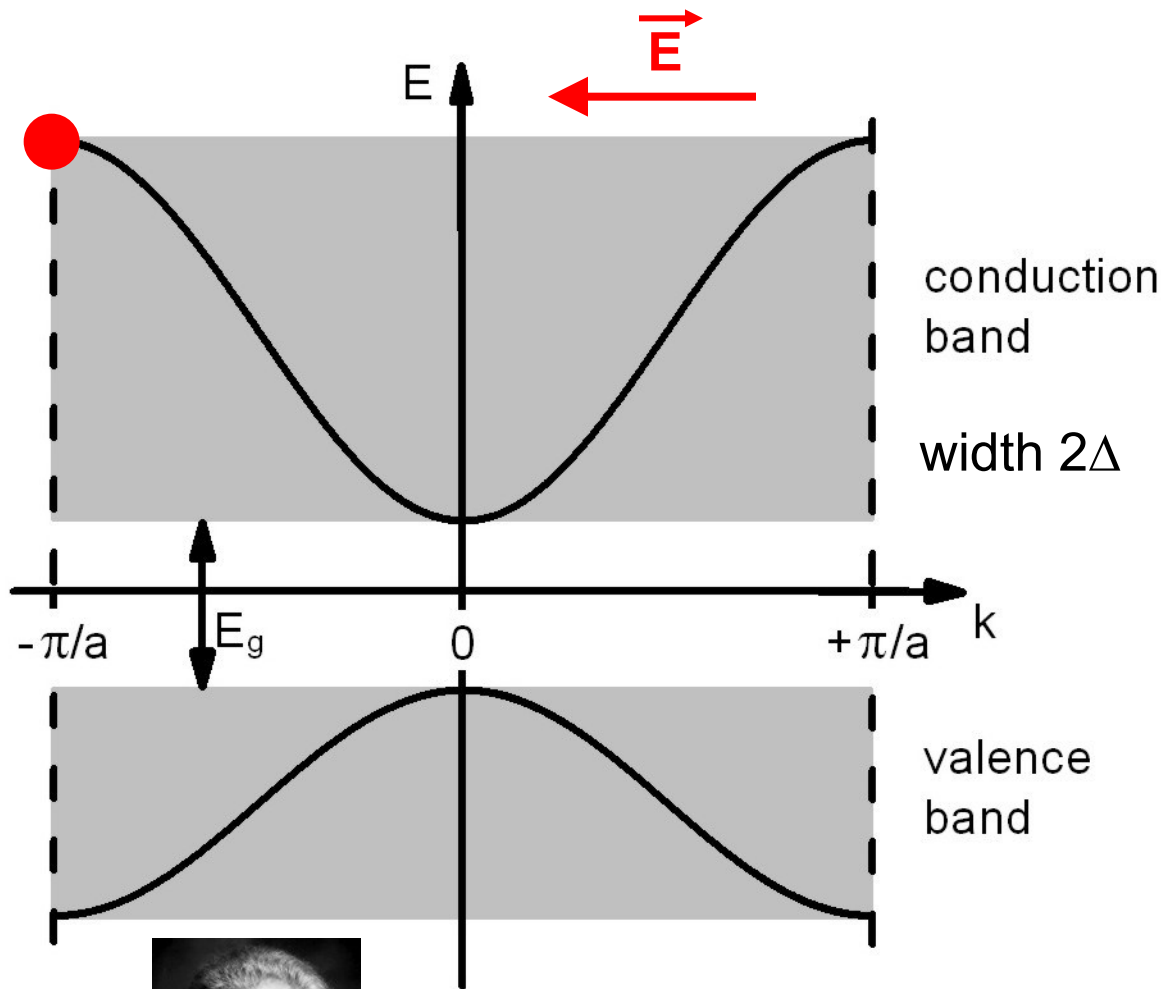


Clarence Zener,  
Proc. R. Soc.  
London A **145**,  
523 (1934)



Gregory H. Wannier,  
Phys. Rev. **117**,  
432 (1960)

# Bloch oscillations in bulk solids



Bloch energy

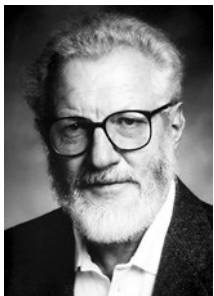
$$\hbar\Omega_B = aeE$$

Bloch period

$$T_B = \frac{h}{aeE}$$

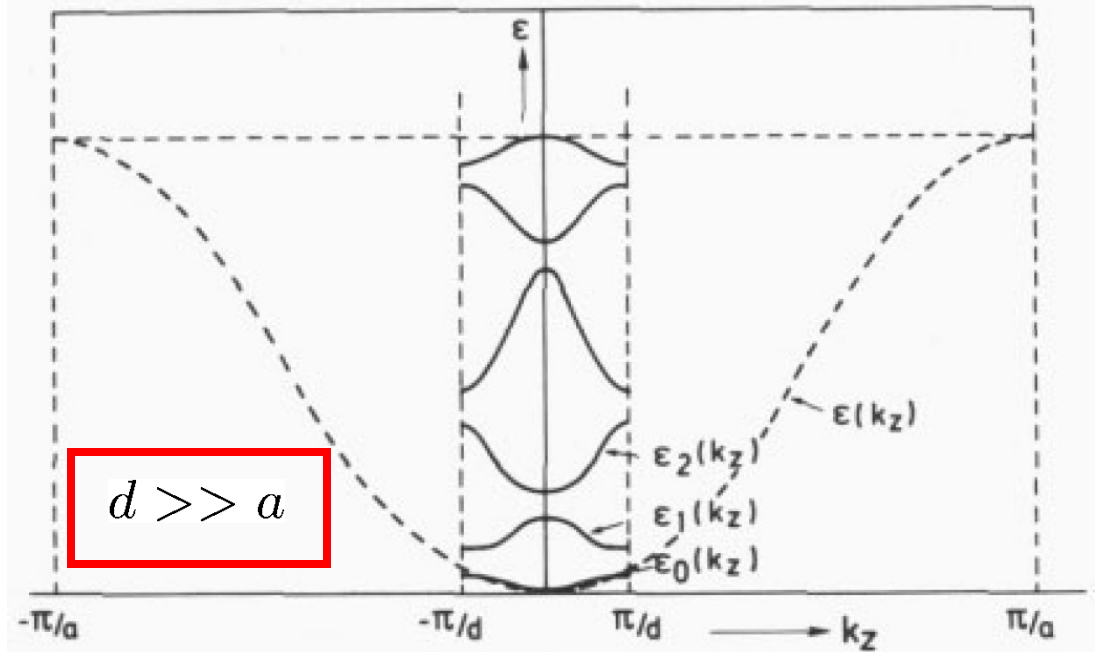
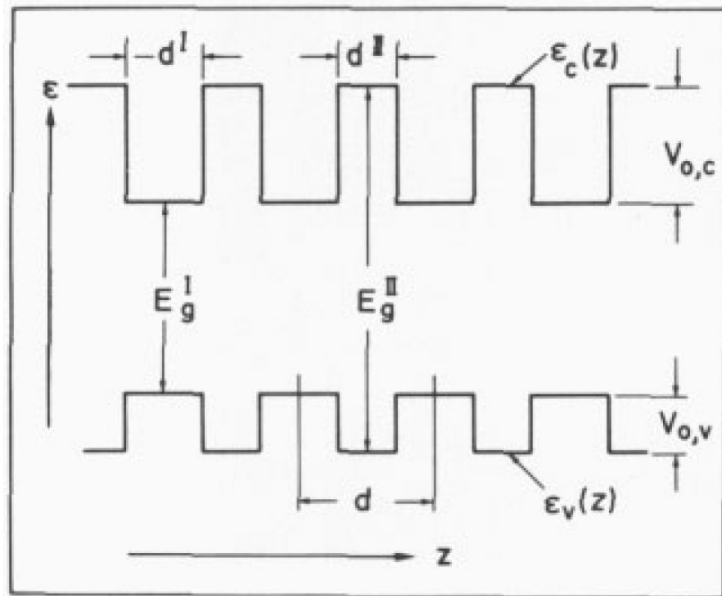
real-space oscillation diameter

$$L_B = \frac{2\Delta}{eE}$$



Herbert Kroemer's Nobel Prize autobiography (2000):  
"... it became obvious that the huge fields required for Bloch oscillations in a **bulk** semiconductor could never be reached."

# Bloch oscillations in semiconductor superlattices



from G. H. Döhler, *Physica Scripta* **24**, 430 (1981)

Bloch energy  $\hbar\Omega_B = deE$

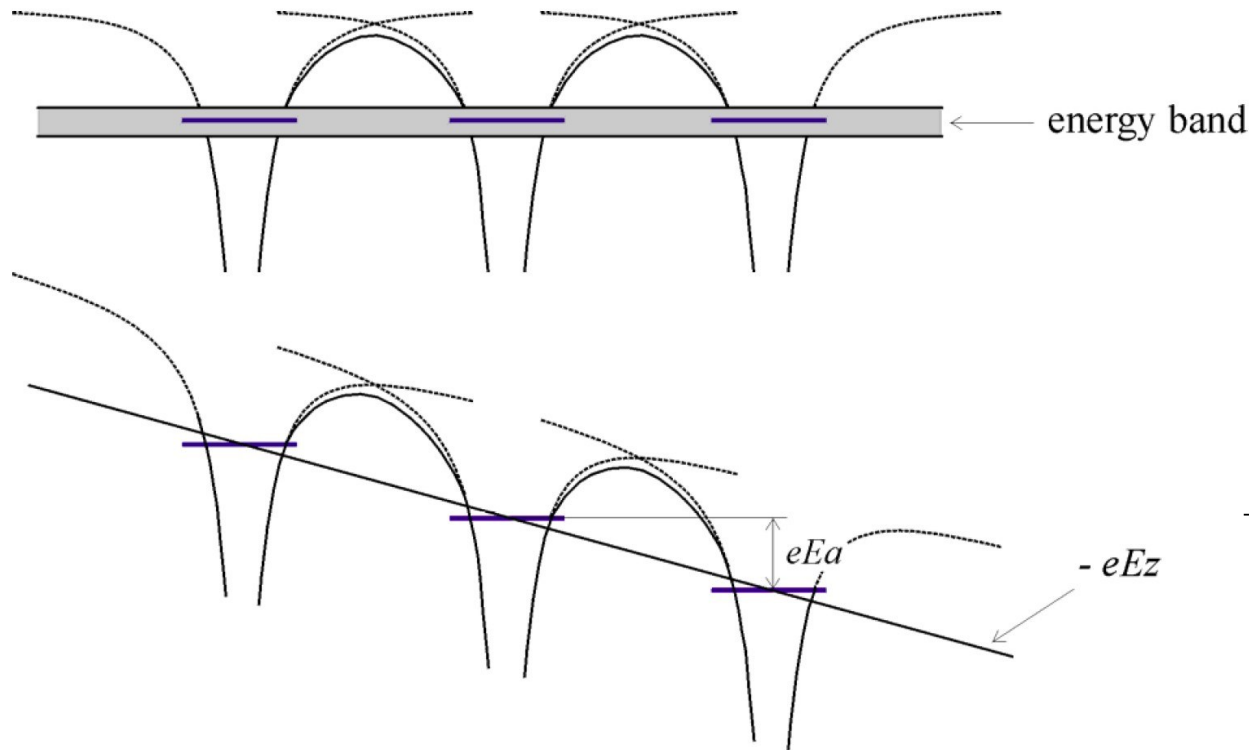
Bloch period  $T_B = \frac{h}{deE}$



L. Esaki *et al.*, *IBM J. Res. Dev.* **14**, 61 (1970):

"If the electron scattering time is sufficiently long, electrons will undergo rf oscillation due to the reflection at the minizone boundaries, the so-called "Bloch oscillation." "

# Wannier-Stark ladders in solids



Wannier-Stark ladder  
 $E_m = E_{\text{ref}} + m a e \tilde{E}_0$   
 $m = 0, \pm 1, \pm 2, \dots$

electron wave packet is **superposition of Wannier-Stark states**,  
**quantum beating** between these states are **Bloch oscillations**

G. H. Wannier, "Wave Functions and Effective Hamiltonian for Bloch electrons in an Electric Field", Phys. Rev. **117**, 432 (1960)

# Equivalence of Bloch-oscillation and Wannier-Stark pictures

Hamiltonian of the system

$$\left[ \frac{\left(-i\hbar\nabla_{\mathbf{r}} - \frac{e}{c}\mathbf{A}(\mathbf{r}, t)\right)^2}{2m_0} + e\varphi(\mathbf{r}, t) + V^{\text{lat}}(\mathbf{r}) \right] \phi_n(\mathbf{r}) = \epsilon_n \phi_n(\mathbf{r})$$

vector-potential gauge:  $\mathbf{A}(\mathbf{r}, t) = -c \int_{t_0}^t \mathbf{E}(t') dt' , \quad \varphi(\mathbf{r}, t) = 0$

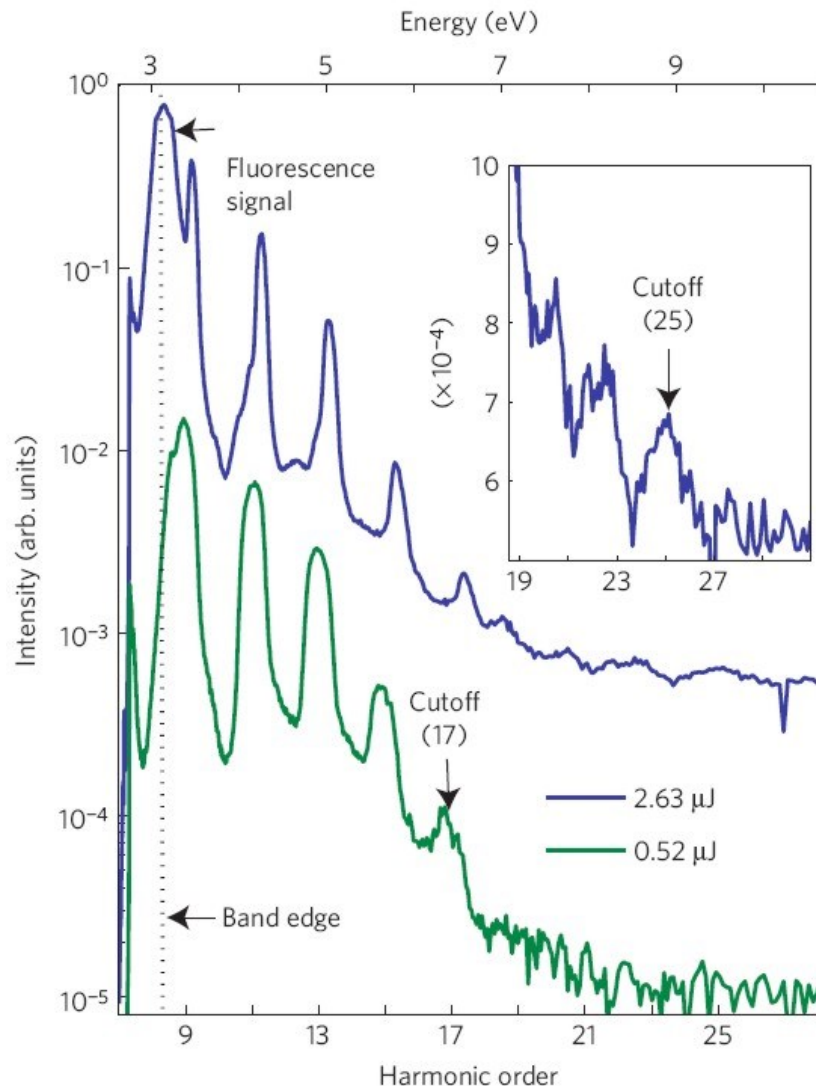
**Bloch-oscillation picture**

scalar-potential gauge:  $\mathbf{A}(\mathbf{r}, t) = 0 , \quad \varphi(\mathbf{r}, t) = -\mathbf{E}(t) \cdot \mathbf{r}$

**Wannier-Stark picture**

total equivalence of the Bloch-oscillation and Wannier-Stark pictures, i.e., the often so-called “semiclassical Bloch picture” is on the contrary a **rigorous quantum-mechanical result** (Fausto Rossi, 1997)

# mid-IR-driven HHG from bulk ZnO



S. Ghimire *et al.*,  
Nature Physics **7**, 138 (2011);  
PRL **107**, 167407 (2011)  
**PRA 107, 167407 (2012)**

500- $\mu\text{m}$ -thin ZnO crystal

9-cycle-long MIR pulses  
( $\sim 100$ -fs  $3.25\text{-}\mu\text{m}$   $0.38\text{-eV}$   
pulses with up to  $2.63\text{ }\mu\text{J}$   
energy, yielding a focused  
field strength of  $6\text{ V/nm}$ )

Bloch HHG up to 25th  
order extending to  $>9.5\text{ eV}$

J. P. Marangos, Nature Physics **7**, 97  
(2011): "An important question not yet  
addressed is whether the harmonic  
emission retains a subfemtosecond  
character; that is, is it confined only to  
certain moments within the optical cycle?  
The observed bandwidth of the emission  
( $\sim 9\text{ eV}$ ) is sufficient to support  
subfemtosecond pulses."